Eur. Phys. J. B **6**, 123–131 (1998)

THE EUROPEAN PHYSICAL JOURNAL B

Self-consistent calculation of electrostatic force for two kinds of mesoscopic surface structures

Z.-Y. Li[1,a], B.-Y. Gu[1,2], and G.-Z. Yang[1,2]

[1] Institute of Physics, Chinese Academy of Sciences, P.O. Box 603, Beijing 100080, P.R. China
[2] CCAST (World Laboratory), P.O. Box 8730, Beijing 100080, P.R. China

Received: 26 March 1998 / Accepted: 9 June 1998

Abstract. The scanning electrostatic force microscopy (SEFM) can acquire information of surface structures in a non-contact way. We calculate the electrostatic force between the charged tip and polarized surface structure in SEFM in the framework of self-consistent integral equation formalism (SCIEF), incorporating the image method to treat the electrostatic coupling of substrate and tip. We consider two kinds of surface structures, one is the topographic structure on the surface, the other is the dielectric structure embedded in the substrate. The force pattern of the topographic structure shows a protrusion around the surface structure. However, the force pattern displays a hollow around an embedded structure with a dielectric constant less than that of substrate medium. For an embedded structure with a larger dielectric constant, the force pattern exhibits a protrusion, and the force signal is much weaker than that of the topographic structure. Therefore, it is expected that one may identify these surface structures from the pure electrostatic force information in SEFM. The force signal of the densely arranged dielectric pads is simply the superposition of force signal of each pad individually, the interference effect of electric field is not remarkable.

PACS. 61.16.Ch Scanning probe microscopy: scanning tunneling, atomic force, scanning optical, magnetic force, etc. – 41.20.Cv Electrostatics; Poisson and Laplace equations, boundary-value problems – 68.35.Bs Surface structure and topography

1 Introduction

The scanning tunneling microscopy (STM) and the scanning force microscopy (SFM) have proven to be the powerful ways to collect information of surface structures [1–3]. When imaging soft or weakly bound material such as liquid adsorbates, polymers and biological samples, various operating principles of SFM were proposed and the SFM's are operated in noncontact mode to reduce surface destruction. The scanning electrostatic force microscopy (SEFM) can be utilized to perform noncontact imaging of both conducting and insulating materials because electrostatic force (Coulomb interaction) possesses a much longer interaction range comparing with the van der Waals force in atomic force microscopy (AFM) and tunneling current in STM. Such an instrument (SEFM) has been applied to image thin film of water [4,5], ferroelectric crystal [6], and conducting electrode [7].

In SEFM a bias voltage is applied to a conductive AFM tip with respect to a remote electrode, for example, the sample holder [4]. The strong electric field around the charged tip induces a polarization inside nearby the sample. Because of the long-range nature of electrostatic interaction, the force between the charged tip and polarized sample can be detected at a distance of several hundreds of angstroms.

In order to extract the information of surface structure from the electrostatic force pattern, the distribution of electrostatic field around the mesoscopic and nanometric surface structures is desired to be known. It requires to solve Poisson equation satisfied by the local electric field, incorporating the match of boundary conditions at each interface of the system including the sample, tip, and substrate. This is a relatively difficult task for the sample with a complex profile and an arbitrarily dielectric distribution. However, a general solution can be acquired in terms of the self-consistent integral equation formalism (SCIEF) as this approach avoids the complicated matching procedure of boundary conditions. Such a method has been widely applied in scattering of electromagnetic wave [8,9] and near field optics [10,11]. More recently, we have utilized this method to treat the electrostatic problem for mesoscopic surface structure in SEFM [12].

In this work we consider two kinds of surface structures in SEFM. One is the topographic structure lying on the surface, the other is the dielectric structure embedded in the substrate and having a different dielectric constant from that of the substrate medium. We calculate

[a] e-mail: wangxh@aphy01.iphy.ac.cn

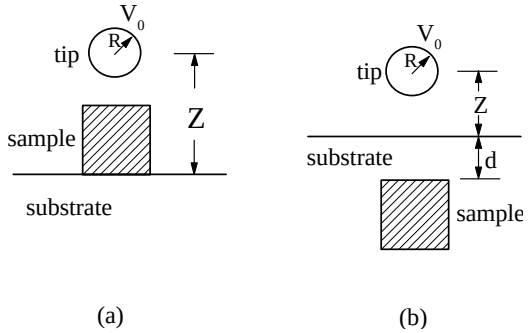

Fig. 1. The schematic configuration of SEFM. (a) Topographic surface structure; (b) embedded dielectric structure. The tip has a bias voltage of $V_0 = 5$ V and a radius of $R = 50$ nm. The dielectric constant of substrate is $\epsilon_s = 2.5$.

the distributions of electric field and the electrostatic force exerting on the scanning tip of SEFM in the framework of SCIEF in the real space representation. Comparing the electrostatic force pattern for these two kinds of surface structures, we can obtain more detailed and clearer understanding on the relationship between the force pattern and the surface structure in SEFM.

This paper is arranged as follows. In Section 2 the technique of Green's function and image method are combined to derive the self-consistent integral equation satisfied by the electric field of the complex system for two kinds of surface structures. In Section 3 we calculate the electrostatic force patterns for a mesoscopic dielectric cubic pad lying on the surface and embedded in the substrate medium, respectively. We also investigate the interference effect of electrostatic force signal between adjacent sample particles. A brief conclusion is made in Section 4.

2 Real-space self-consistent method for SEFM

In a simplified way, the conductive AFM tip in SEFM is modeled as a conductive sphere with a radius of R and a potential of V_0. There are two kinds of surface structures, one is a topographic surface structure lying on the surface, the other is a dielectric surface structure embedded in the substrate medium and having a different dielectric constant from that of the substrate medium. The schematic configuration of SEFM is displayed in Figures 1a and b for these two kinds of surface structures, respectively. When such a spherical tip is scanned above a perfect semiinfinite substrate with a dielectric constant ϵ_s, the electric field $\mathbf{E}_0(\mathbf{r})$ in the space above and below the interface can be derived analytically in terms of the standard image charge method [13]. The charge density distribution $\sigma_0(\mathbf{r})$ on the surface of tip can be evaluated. Thus the electrostatic force $\mathbf{F}_0$ between the tip and the substrate can be calculated. The sample embedded in this electric field is polarized and such a polarization serves as the secondary field source. The elementary charge distribution on the surface of tip is then modified, and the local electric field is perturbed. Finally the secondary and elementary field source reach a self-consistent distribution which is the solution of the complex electrostatic problem in SEFM. From the self-consistent electric field of the complex system, one can calculate the electrostatic force exerting on the tip straightforwardly.

2.1 Self-consistent equations for topographic surface structure

The self-consistent local field inside the sample $\mathbf{E}(\mathbf{r})$ induces a polarization $\mathbf{P}(\mathbf{r}) = [\epsilon(\mathbf{r}) - 1]\mathbf{E}(\mathbf{r})$, which serves as the secondary field source. Here $\epsilon(\mathbf{r})$ is the dielectric distribution of the sample. Taking into account the coupling of the substrate and the conductive spherical tip, the local field $\mathbf{E}(\mathbf{r})$ and polarization $\mathbf{P}(\mathbf{r})$ both are modified. The electric field due to the polarization $\mathbf{P}(\mathbf{r})$ can be derived through the electrostatic potential [13,14]. More conveniently, we prefer to employ the scattering theory of electromagnetic wave. According to this theory, the secondary field induced by the polarization $\mathbf{P}(\mathbf{r})$ reads [11]

$$\mathbf{E}_s(\mathbf{r}) = \int_{V_s} (\nabla\nabla + k^2) G(\mathbf{r}, \mathbf{r}'; k) \cdot \mathbf{P}(\mathbf{r}') d^3\mathbf{r}', \qquad (1)$$

where the Green's function is given by

$$G(\mathbf{r}, \mathbf{r}'; k) = \frac{\exp(ik|\mathbf{r} - \mathbf{r}'|)}{4\pi|\mathbf{r} - \mathbf{r}'|},$$

and k is the wavenumber of electromagnetic wave in free space, V_s the region of sample scatterer. This formula is valid in the whole space, *i.e.*, inside and outside the sample. Let $k = 0$, it reduces to an electrostatic case and the formula reads

$$\mathbf{E}_s(\mathbf{r}) = \int_{V_s} \mathbf{g}_0(\mathbf{r}, \mathbf{r}') \cdot \mathbf{P}(\mathbf{r}') d^3\mathbf{r}', \qquad (2)$$

where the dyadic Green's function $\mathbf{g}_0(\mathbf{r}, \mathbf{r}') = \nabla\nabla G(\mathbf{r}, \mathbf{r}')$ has the matrix element as

$$g_0^{ij}(\mathbf{r}, \mathbf{r}') = \frac{\partial^2}{\partial x_i x_j} G(\mathbf{r}, \mathbf{r}'), \qquad x_i, x_j = x, y, z,$$

with the Green's function of the Coulomb interaction

$$G(\mathbf{r}, \mathbf{r}') = \frac{1}{4\pi|\mathbf{r} - \mathbf{r}'|}.$$

The coupling of the substrate and tip can be evaluated through the image method. It requires us to derive the image polarization distribution of $\mathbf{P}(\mathbf{r})$ with respect to the substrate and tip. For convenience, we first treat the case of time-dependent electromagnetic field, then extrapolate to the limit of electrostatic field which is just the special case of electromagnetic field with zero frequency.

Assume that the polarized charge $\rho(\mathbf{r})d^3\mathbf{r}$ oscillates with a velocity $\mathbf{v}(\mathbf{r})$ and produces the polarized current

$\mathbf{j}(\mathbf{r})d^3\mathbf{r} = \rho(\mathbf{r})\mathbf{v}(\mathbf{r})d^3\mathbf{r}$. Such a polarized current induces an image current with respect to the substrate as

$$\begin{aligned}\mathbf{j}_{is}(\mathbf{r}_{is})d^3\mathbf{r}_{is} &= \rho_{is}(\mathbf{r}_{is})\mathbf{v}_{is}(\mathbf{r}_{is})d^3\mathbf{r}_{is}\\ &= -\gamma_1\rho(\mathbf{r})[v_x(\mathbf{r}), v_y(\mathbf{r}), -v_z(\mathbf{r})]d^3\mathbf{r}\\ &= -\gamma_1[j_x(\mathbf{r}), j_y(\mathbf{r}), -j_z(\mathbf{r})]d^3\mathbf{r}, \qquad (3)\end{aligned}$$

where $\gamma_1 = (\epsilon_s - 1)/(\epsilon_s + 1)$ is the image factor, and $\mathbf{r}_{is}$ is the image of $\mathbf{r}$ with respect to the substrate. The time-dependent polarized current $\mathbf{j}(\mathbf{r})$ is related to the polarization $\mathbf{P}(\mathbf{r})$ as $\mathbf{j}(\mathbf{r}) = -i\omega\epsilon_0\mathbf{P}(\mathbf{r})$, where ω is the frequency of oscillating charge [11]. Then the image polarization $\mathbf{P}_{is}(\mathbf{r}_{is})$ is related to $\mathbf{P}(\mathbf{r})$ as

$$\mathbf{P}_{is}(\mathbf{r}_{is})d^3\mathbf{r}_{is} = -\gamma_1[P_x(\mathbf{r}), P_y(\mathbf{r}) - P_z(\mathbf{r})]d^3\mathbf{r}. \qquad (4)$$

One can find the image polarization with respect to the semiinfinite substrate $\mathbf{P}_{is}(\mathbf{r}_{is})$ is anti-parallel in the x and y axes, and parallel in the z axis with the secondary polarization $\mathbf{P}(\mathbf{r})$.

To obtain the image current with respect to the conductive spherical tip $\mathbf{j}_{it}$, we first investigate the oscillating velocity of image polarized charge. According to standard image method [13], for the case of a conductive sphere with a fixed potential, the polarized charge $\rho(\mathbf{r})d^3\mathbf{r}$ induces an image charge $\rho_{it}(\mathbf{r}_{it})d^3\mathbf{r}_{it} = -\alpha(\mathbf{r})\rho(\mathbf{r})d^3\mathbf{r}$ inside the sphere. The image charge is located at the image position $\mathbf{r}_{it} = \alpha^2(\mathbf{r})\mathbf{r}$ with the image factor $\alpha(\mathbf{r}) = R/\mid\mathbf{r}\mid$. The oscillating velocity is

$$\mathbf{v}_i(\mathbf{r}_{it}) = \frac{d\mathbf{r}_{it}}{dt} = \frac{d}{dt}[\alpha^2(\mathbf{r})\mathbf{r}] = \alpha^2(\mathbf{r})\big\{\mathbf{v}(\mathbf{r}) - 2[\hat{\mathbf{r}}\cdot\mathbf{v}(\mathbf{r})]\hat{\mathbf{r}}\big\}, \qquad (5)$$

where $\hat{\mathbf{r}} = \mathbf{r}/|\mathbf{r}|$ denotes a unit vector. Then the image current is

$$\begin{aligned}\mathbf{j}_{it}(\mathbf{r}_{it})d^3\mathbf{r}_{it} &= \rho_{it}(\mathbf{r}_{it})\mathbf{v}_i(\mathbf{r}_{it})d^3\mathbf{r}_{it}\\ &= -\alpha(\mathbf{r})\rho(\mathbf{r})d^3\mathbf{r}\times\alpha^2(\mathbf{r})\big\{\mathbf{v}(\mathbf{r}) - 2[\hat{\mathbf{r}}\cdot\mathbf{v}(\mathbf{r})]\mathbf{r}\big\}\\ &= -\alpha^3(\mathbf{r})\big\{\mathbf{j}(\mathbf{r}) - 2[\hat{\mathbf{r}}\cdot\mathbf{j}(\mathbf{r})]\hat{\mathbf{r}}\big\}d^3\mathbf{r}. \qquad (6)\end{aligned}$$

The corresponding image polarization reads

$$\mathbf{P}_{it}(\mathbf{r}_{it})d^3\mathbf{r}_{it} = -\alpha^3(\mathbf{r})\big\{\mathbf{P}(\mathbf{r}) - 2[\hat{\mathbf{r}}\cdot\mathbf{P}(\mathbf{r})]\hat{\mathbf{r}}\big\}d^3\mathbf{r}. \qquad (7)$$

The electric field induced by the two image polarization distributions $\mathbf{P}_{is}(\mathbf{r}_{is})$ and $\mathbf{P}_{it}(\mathbf{r}_{it})$ can be evaluated straightforwardly according to equation (2). The electric field modified by the substrate can be expressed as

$$\begin{aligned}\mathbf{E}_{is}(\mathbf{r}) &= \int_{V_{is}}\mathbf{g}_0(\mathbf{r},\mathbf{r}'_{is})\cdot\mathbf{P}_{is}(\mathbf{r}'_{is})d^3\mathbf{r}'_{is}\\ &= \int_{V_s}\mathbf{g}_{is}(\mathbf{r},\mathbf{r}')\cdot\mathbf{P}(\mathbf{r}')d^3\mathbf{r}', \qquad (8)\end{aligned}$$

where the dyadic function is given by

$$\mathbf{g}_{is}(\mathbf{r},\mathbf{r}') = -\gamma_1\begin{pmatrix}\frac{\partial^2}{\partial x^2} & \frac{\partial^2}{\partial x\partial y} & -\frac{\partial^2}{\partial x\partial z}\\ \frac{\partial^2}{\partial y\partial x} & \frac{\partial^2}{\partial y^2} & -\frac{\partial^2}{\partial y\partial z}\\ \frac{\partial^2}{\partial z\partial x} & \frac{\partial^2}{\partial z\partial y} & -\frac{\partial^2}{\partial z^2}\end{pmatrix}G(\mathbf{r},\mathbf{r}'_{is})$$

with the coordinate $\mathbf{r}'_{is}$ in the image region of sample with respect to the substrate. The coupling effect of substrate represented by $\mathbf{g}_{is}(\mathbf{r},\mathbf{r}')$ decays cubically with respect to $1/|\mathbf{r}-\mathbf{r}'_{is}|$.

The electric field perturbed by the conductive spherical tip reads

$$\begin{aligned}\mathbf{E}_{it}(\mathbf{r}) &= \int_{V_{it}}\mathbf{g}_0(\mathbf{r},\mathbf{r}'_{it})\cdot\mathbf{P}_{it}(\mathbf{r}'_{it})d^3\mathbf{r}'_{it}\\ &= \int_{V_s}\mathbf{g}_{it}(\mathbf{r},\mathbf{r}')\cdot\mathbf{P}(\mathbf{r}')d^3\mathbf{r}', \qquad (9)\end{aligned}$$

where the dyadic function $\mathbf{g}_{it}(\mathbf{r},\mathbf{r}')$ has the matrix element as

$$\begin{aligned}g_{it}^{ij}(\mathbf{r},\mathbf{r}') = -\alpha^3(\mathbf{r}')\big[&\frac{\partial^2}{\partial x_i x_j}G(\mathbf{r},\mathbf{r}'_{it})\\ &-2\sum_k\frac{\partial^2}{\partial x_i x_k}G(\mathbf{r},\mathbf{r}'_{it})\hat{x}_k\hat{x}_j\big],\\ x_i, x_j, x_k = x, y, z, &\quad \hat{x}_i,\hat{x}_j,\hat{x}_k = \hat{x},\hat{y},\hat{z},\end{aligned}$$

with the coordinate $\mathbf{r}'_{it}$ in the image region of sample with respect to the tip. The dyadic function $\mathbf{g}_{it}(\mathbf{r},\mathbf{r}')$ is cubically proportional to the image factor α, thus it also decays cubically with respect to $1/|\mathbf{r}-\mathbf{r}'_{it}|$.

So far we have yielded the local electric field polarizing the sample, which is composed of four terms: the unperturbed field $\mathbf{E}_0(\mathbf{r})$, the field $\mathbf{E}_s(\mathbf{r})$ induced by the polarization of sample, and the coupled fields $\mathbf{E}_{is}(\mathbf{r})$ and $\mathbf{E}_{it}(\mathbf{r})$, which are induced by the image polarization with respect to the substrate and tip, respectively. The rigorous electric local field should include the contributions of the coupling of tip with the image polarization $\mathbf{P}_{is}(\mathbf{r}_{is})$ and the coupling of the substrate with the image polarization $\mathbf{P}_{it}(\mathbf{r}_{it})$. Such multiple image contributions are proportional to the multiplication of two image effects denoted by $\mathbf{g}_{is}$ and $\mathbf{g}_{it}$. Considering the fast decaying feature of these two dyadic functions, the multiple image contributions are small and can be neglected. Then we have

$$\mathbf{E}(\mathbf{r}) = \mathbf{E}_0(\mathbf{r}) + \mathbf{E}_s(\mathbf{r}) + \mathbf{E}_{is}(\mathbf{r}) + \mathbf{E}_{it}(\mathbf{r}). \qquad (10)$$

Inserting equations (2, 8, 9) into equation (10), we can derive the self-consistent integral equation satisfied

by the local field $\mathbf{E}(\mathbf{r})$ as

$$\begin{aligned}\mathbf{E}(\mathbf{r}) &= \mathbf{E}_0(\mathbf{r}) + \int_{V_s} \mathbf{g}_0(\mathbf{r},\mathbf{r}')\cdot\mathbf{P}(\mathbf{r}')d^3\mathbf{r}' \\ &\quad + \int_{V_s} \mathbf{g}_{is}(\mathbf{r},\mathbf{r}')\cdot\mathbf{P}(\mathbf{r}')d^3\mathbf{r}' + \int_{V_s} \mathbf{g}_{it}(\mathbf{r},\mathbf{r}')\cdot\mathbf{P}(\mathbf{r}')d^3\mathbf{r}' \\ &= \mathbf{E}_0(\mathbf{r}) + \int_{V_s} \mathbf{g}(\mathbf{r},\mathbf{r}')\cdot\mathbf{P}(\mathbf{r}')d^3\mathbf{r}' \\ &= \mathbf{E}_0(\mathbf{r}) + \int_{V_s} \mathbf{g}(\mathbf{r},\mathbf{r}')\cdot[\epsilon(\mathbf{r}')-1]\mathbf{E}(\mathbf{r}')d^3\mathbf{r}', \qquad (11)\end{aligned}$$

where the dyadic function of the complex system is given by

$$\mathbf{g}(\mathbf{r},\mathbf{r}') = \mathbf{g}_0(\mathbf{r},\mathbf{r}') + \mathbf{g}_{is}(\mathbf{r},\mathbf{r}') + \mathbf{g}_{it}(\mathbf{r},\mathbf{r}').$$

2.2 Self-consistent integral equation for embedded dielectric structure

The self-consistent integral equation for embedded dielectric structure can be deduced in the same framework as the case of the topographic surface structure.

The secondary field source induced by the charged tip above the surface now is $\mathbf{P}(\mathbf{r}) = [\epsilon(\mathbf{r}) - \epsilon_s]\mathbf{E}(\mathbf{r})$ [11], where $\epsilon(\mathbf{r})$ is the dielectric distribution of the embedded structure, $\mathbf{E}(\mathbf{r})$ is the local electric field. The secondary field induced by this polarization is

$$\mathbf{E}_s(\mathbf{r}) = \int_{V_s} \mathbf{g}_0(\mathbf{r},\mathbf{r}')\cdot\mathbf{P}(\mathbf{r}')d^3\mathbf{r}', \qquad (12)$$

where the dyadic Green's function is

$$\mathbf{g}_0(\mathbf{r},\mathbf{r}') = \frac{1}{\epsilon_s}\nabla\nabla G(\mathbf{r},\mathbf{r}'), \quad \text{with} \quad G(\mathbf{r},\mathbf{r}') = \frac{1}{4\pi|\mathbf{r}-\mathbf{r}'|}.$$

The coefficient $1/\epsilon_s$ in $\mathbf{g}_0(\mathbf{r},\mathbf{r}')$ is due to the screened Coulomb interaction in dielectric medium.

The electric field due to the coupling of substrate can be attributed to the image polarization

$$\mathbf{P}_{is}(\mathbf{r}_{is})d^3\mathbf{r}_{is} = \gamma_1[P_x(\mathbf{r}), P_y(\mathbf{r}) - P_z(\mathbf{r})]d^3\mathbf{r}. \qquad (13)$$

Such a modified field reads

$$\mathbf{E}_{is}(\mathbf{r}) = \int_{V_s} \mathbf{g}_{is}(\mathbf{r},\mathbf{r}')\cdot\mathbf{P}(\mathbf{r}')d^3\mathbf{r}', \qquad (14)$$

where the dyadic function is

$$\mathbf{g}_{is}(\mathbf{r},\mathbf{r}') = \frac{\gamma_1}{\epsilon_s}\begin{pmatrix} \frac{\partial^2}{\partial x^2} & \frac{\partial^2}{\partial x\partial y} & -\frac{\partial^2}{\partial x\partial z} \\ \frac{\partial^2}{\partial y\partial x} & \frac{\partial^2}{\partial y^2} & -\frac{\partial^2}{\partial y\partial z} \\ \frac{\partial^2}{\partial z\partial x} & \frac{\partial^2}{\partial z\partial y} & -\frac{\partial^2}{\partial z^2} \end{pmatrix} G(\mathbf{r},\mathbf{r}'_{is})$$

with the coordinate $\mathbf{r}'_{is}$ in the image region of sample with respect to the substrate.

The electric field coupled by the spherical conductive tip can be attributed to the image polarization as

$$\mathbf{P}_{it}(\mathbf{r}_{it})d^3\mathbf{r}_{it} = -\gamma_2\alpha^3(\mathbf{r})\{\mathbf{P}(\mathbf{r}) - 2[\hat{\mathbf{r}}\cdot\mathbf{P}(\mathbf{r})]\hat{\mathbf{r}}\}d^3\mathbf{r}, \qquad (15)$$

where $\gamma_2 = 2/(1+\epsilon_s)$ is the image factor describing the response of electrostatic field below an interface to the source above the interface. Then the electric field perturbed by the conductive spherical tip reads

$$\mathbf{E}_{it}(\mathbf{r}) = \int_{V_s} \mathbf{g}_{it}(\mathbf{r},\mathbf{r}')\cdot\mathbf{P}(\mathbf{r}')d^3\mathbf{r}', \qquad (16)$$

where the dyadic function $\mathbf{g}_{it}(\mathbf{r},\mathbf{r}')$ has the matrix element as

$$\begin{aligned} g_{it}^{ij}(\mathbf{r},\mathbf{r}') = -\gamma_2^2\alpha^3(\mathbf{r}')\Big[&\frac{\partial^2}{\partial x_i x_j}G(\mathbf{r},\mathbf{r}'_{it}) \\ &-2\sum_k \frac{\partial^2}{\partial x_i x_k}G(\mathbf{r},\mathbf{r}'_{it})\hat{x}_k\hat{x}_j\Big], \end{aligned}$$

$$x_i, x_j, x_k = x, y, z, \quad \hat{x}_i, \hat{x}_j, \hat{x}_k = \hat{x}, \hat{y}, \hat{z},$$

with the coordinate $\mathbf{r}'_{it}$ in the image region of sample with respect to the tip.

The coupling interaction dyadic functions denoted by $\mathbf{g}_{is}$ and $\mathbf{g}_{it}$ also decay inverse-cubically with respect to the source-field distance. Taking into account this fast decaying character, the multiple image contributions can be neglected, similar to the case of the topographic surface structure. Then we obtain the self-consistent integral equation as

$$\begin{aligned}\mathbf{E}(\mathbf{r}) &= \mathbf{E}_0(\mathbf{r}) + \mathbf{E}_s(\mathbf{r}) + \mathbf{E}_{is}(\mathbf{r}) + \mathbf{E}_{it}(\mathbf{r}) \\ &= \mathbf{E}_0(\mathbf{r}) + \int_{V_s} \mathbf{g}_0(\mathbf{r},\mathbf{r}')\cdot\mathbf{P}(\mathbf{r}')d^3\mathbf{r}' \\ &\quad + \int_{V_s} \mathbf{g}_{is}(\mathbf{r},\mathbf{r}')\cdot\mathbf{P}(\mathbf{r}')d^3\mathbf{r}' + \int_{V_s} \mathbf{g}_{it}(\mathbf{r},\mathbf{r}')\cdot\mathbf{P}(\mathbf{r}')d^3\mathbf{r}' \\ &= \mathbf{E}_0(\mathbf{r}) + \int_{V_s} \mathbf{g}(\mathbf{r},\mathbf{r}')\cdot\mathbf{P}(\mathbf{r}')d^3\mathbf{r}' \\ &= \mathbf{E}_0(\mathbf{r}) + \int_{V_s} \mathbf{g}(\mathbf{r},\mathbf{r}')\cdot[\epsilon(\mathbf{r}')-\epsilon_s]\mathbf{E}(\mathbf{r}')d^3\mathbf{r}', \qquad (17)\end{aligned}$$

where the dyadic function of the complex system for the embedded surface structure is given by

$$\mathbf{g}(\mathbf{r},\mathbf{r}') = \mathbf{g}_0(\mathbf{r},\mathbf{r}') + \mathbf{g}_{is}(\mathbf{r},\mathbf{r}') + \mathbf{g}_{it}(\mathbf{r},\mathbf{r}').$$

2.3 Formulas for numerical simulations

The common method for solving the integral equations (11, 17) is to discretize the region of sample into a number of sampling cells, and then solve a set of linear simultaneous equations for the fields at the discretized sampling cells. Let $\mathbf{E}(\mathbf{r}_i)$ denote the field at the ith sampling cell. Then equation (11) leads to a set of linear simultaneous equations as

$$\mathbf{E}(\mathbf{r}_i) = \mathbf{E}_0(\mathbf{r}_i) + \sum_{j=1}^{n} W_j\mathbf{g}(\mathbf{r}_i,\mathbf{r}_j)[\epsilon(\mathbf{r}_j)-1]\mathbf{E}(\mathbf{r}_j), \qquad (18)$$

$$\mathbf{f}(\mathbf{r},\mathbf{r}') = \begin{pmatrix} W_1[\epsilon(\mathbf{r}_1)-1]\mathbf{g}(\mathbf{r}_1,\mathbf{r}_1) & W_2[\epsilon(\mathbf{r}_2)-1]\mathbf{g}(\mathbf{r}_1,\mathbf{r}_2) & \cdots & W_n[\epsilon(\mathbf{r}_n)-1]\mathbf{g}(\mathbf{r}_1,\mathbf{r}_n) \\ W_1[\epsilon(\mathbf{r}_1)-1]\mathbf{g}(\mathbf{r}_2,\mathbf{r}_1) & W_2[\epsilon(\mathbf{r}_2)-1]\mathbf{g}(\mathbf{r}_2,\mathbf{r}_2) & \cdots & W_n[\epsilon(\mathbf{r}_n)-1]\mathbf{g}(\mathbf{r}_2,\mathbf{r}_n) \\ \cdots & \cdots & \cdots & \cdots \\ \cdots & \cdots & \cdots & \cdots \\ W_1[\epsilon(\mathbf{r}_1)-1]\mathbf{g}(\mathbf{r}_n,\mathbf{r}_1) & W_2[\epsilon(\mathbf{r}_2)-1]\mathbf{g}(\mathbf{r}_n,\mathbf{r}_2) & \cdots & W_n[\epsilon(\mathbf{r}_n)-1]\mathbf{g}(\mathbf{r}_n,\mathbf{r}_n) \end{pmatrix}.$$

where W_j represents the volume of the jth sampling cell and n is the total number of sampling cells. The set of unknown vectors $\{\mathbf{E}(\mathbf{r}_i,\omega)\}$ can be determined by the standard algebraic manipulation.

Introducing two supervectors

$$\mathbf{E} = \{\mathbf{E}(\mathbf{r}_1);\mathbf{E}(\mathbf{r}_2);\cdots;\mathbf{E}(\mathbf{r}_n)\}$$

and

$$\mathbf{E}_0 = \{\mathbf{E}_0(\mathbf{r}_1);\mathbf{E}_0(\mathbf{r}_2);\cdots;\mathbf{E}_0(\mathbf{r}_n)\}$$

as well as the $(3n\times 3n)$ matrix

$$\mathbf{g} = \mathbf{I} - \mathbf{f}(\mathbf{r},\mathbf{r}'),$$

where $\mathbf{I}$ represents an identity matrix with $3n\times 3n$ dimension, and $\mathbf{f}(\mathbf{r},\mathbf{r}')$ is a $(3n\times 3n)$ matrix defined by

See equation above.

Equation (18) then becomes

$$\mathbf{E}_0 = \mathbf{g}\mathbf{E}. \tag{19}$$

When the dimension of the matrix $\mathbf{g}$ takes an appropriate value, then, it is possible to give an accurate numerical solution for the field distribution contained in the supervector $\mathbf{E}(\mathbf{r})$ in the self-consistent form.

The integral equation (17) for the embedded dielectric structure can be numerically solved in the same way as equation (11) for topographic surface structure. The local electric field can be obtained in the self-consistent form.

2.4 Electrostatic forces exerting on the tip

When the local electric field of sample $\mathbf{E}(\mathbf{r})$ is solved self-consistently, the secondary field induced by the polarization of sample $\mathbf{P}(\mathbf{r})$ can be derived straightforwardly. In the case of the topographic surface structure it is

$$\begin{aligned}\mathbf{E}(\mathbf{r}) &= \mathbf{E}_s(\mathbf{r}) + \mathbf{E}_{is}(\mathbf{r}) \\ &= \int_{V_s} \mathbf{g}_0(\mathbf{r},\mathbf{r}')\cdot\mathbf{P}(\mathbf{r}')d^3\mathbf{r}' + \int_{V_s} \mathbf{g}_{is}(\mathbf{r},\mathbf{r}')\cdot\mathbf{P}(\mathbf{r}')d^3\mathbf{r}' \\ &= \int_{V_s} [\mathbf{g}_0(\mathbf{r},\mathbf{r}') + \mathbf{g}_{is}(\mathbf{r},\mathbf{r}')]\cdot[\epsilon(\mathbf{r}')-1]\mathbf{E}(\mathbf{r}')d^3\mathbf{r}'. \end{aligned} \tag{20}$$

Here we also neglect the coupling of substrate with the image polarization $\mathbf{P}_{it}(\mathbf{r})$. In the discretized form the field is

$$\mathbf{E}(\mathbf{r}) = \sum_{j=1}^{n} W_j[\mathbf{g}_0(\mathbf{r},\mathbf{r}_j) + \mathbf{g}_{is}(\mathbf{r},\mathbf{r}_j)][\epsilon(\mathbf{r}_j)-1]\mathbf{E}(\mathbf{r}_j). \tag{21}$$

For the embedded dielectric surface structure, the secondary field induced by the polarization of sample $\mathbf{P}(\mathbf{r})$ reads

$$\begin{aligned}\mathbf{E}(\mathbf{r}) &= \int_{V_s} \mathbf{g}_s(\mathbf{r},\mathbf{r}')\cdot\mathbf{P}(\mathbf{r}')d^3\mathbf{r}' \\ &= \int_{V_s} \mathbf{g}_s(\mathbf{r},\mathbf{r}')\cdot[\epsilon(\mathbf{r}')-\epsilon_s]\mathbf{E}(\mathbf{r}')d^3\mathbf{r}', \end{aligned} \tag{22}$$

where the dyadic functions $\mathbf{g}_s(\mathbf{r},\mathbf{r}')$ is

$$\mathbf{g}_s(\mathbf{r},\mathbf{r}') = \gamma_2\nabla\nabla G(\mathbf{r},\mathbf{r}').$$

In the discretized form the field is

$$\mathbf{E}(\mathbf{r}) = \sum_{j=1}^{n} W_j\mathbf{g}_s(\mathbf{r},\mathbf{r}_j)[\epsilon(\mathbf{r}_j)-\epsilon_s]\mathbf{E}(\mathbf{r}_j). \tag{23}$$

The secondary electric field induced by the surface structure exerts on the surface charge of the tip and induces the additional electrostatic force due to the presence of sample. The additional force $\mathbf{F}_1$ can be calculated by

$$\mathbf{F}_1 = \sum_{i=1}^{m} s_i\mathbf{E}(\mathbf{r}_i)\sigma_0(\mathbf{r}_i), \tag{24}$$

where s_i represents the area of the ith sampling cell, and m is the total number of sampling cells on the surface of tip. The whole electrostatic field $\mathbf{F}$ exerting on the tip is the superposition of the unperturbed force $\mathbf{F}_0$ and the additional force $\mathbf{F}_1$, *i.e.*, $\mathbf{F} = \mathbf{F}_0 + \mathbf{F}_1$.

It is evident that the unperturbed force $\mathbf{F}_0$ does not contain any information of the surface structure, this force only serves as a background force. Thus the surface structural signal of electrostatic force can be defined as the normalized force signal as

$$I = \frac{F_z}{F_0}. \tag{25}$$

Here F_z is the vertical z component of the whole force $\mathbf{F}$, while F_0 is the force in the absence of the sample and is along the z axis. Other horizontal components of $\mathbf{F}$ do not affect the operation of conductive AFM tip, and are thus neglected.

When the tip is scanned above the surface structure, we have to solve the self-consistent integral equations at each observation site. Then we calculate the electrostatic

force and subsequently the normalized force signal according to equation (25). In this way, we can obtain the scanning force pattern, which should reflect the information of surface structure such as topography, geometric size, and dielectricity, *etc.*

3 Numerical simulation results

In our numerical simulations, we choose the geometric and physical parameters as follows: the bias voltage is $V_0 = 5$ V, the radius of tip $R = 50$ nm, and the dielectric constant of the substrate $\epsilon_s = 2.5$.

We first consider a cubic topographic surface structure. The sample has a dielectric constant of $\epsilon = 2.5$ and a sidelength of $a = 100$ nm. Assume that the tip is operated in the constant-height mode and scanned in the observation plane of Z. The three dimensional (3D) perspective views of the normalized force signal at different scanning planes of $Z = 175$, 200, and 225 nm are displayed in Figures 2a, b, and c, respectively. It is evident that the force signal reaches a maximum when the tip is centered right with the sample, and the signal decays rapidly when increasing the tip-sample distance. This is due to the fast decaying feature of electrostatic field induced by the polarized sample. The force signal also decays when the tip deviates from the center position of the sample. The maximum normalized force signal at the three scanning planes are $I_m = 3.14$, 2.11, and 1.65, respectively. Furthermore, the apparent size of sample obtained from the force signal grows larger with the increase of Z. This means that more information of surface structure is lost at a higher scanning plane. If we define such an apparent size as the full width at half maximum of the normalized force signal at a certain scanning plane along the side direction of cube, then the apparent size of the cubic sample is about 140, 160, and 180 nm at the three planes of $Z = 175$, 200, and 225 nm, respectively. The apparent size is approximately linearly proportional to the vertical tip-sample distance.

We next investigate the embedded dielectric structure shown in Figure 1b. We also assume that the sample is a cubic dielectric pad with a sidelength of $a = 100$ nm. Two cases of sample dielectricity should be taken into account, *i.e.*, the sample has a dielectric constant either less or larger than that of substrate medium.

As the first case we assume that a hollow (vacuum) is embedded in the substrate. Then the dielectric constant of sample is $\epsilon = 1.0$. When the tip of SEFM is operated in the constant-height mode and scanned on a certain observation plane of Z, we solve the self-consistent integral equations for the embedded dielectric surface structure at each observation point and then obtain the synthesized electrostatic force pattern. Figures 3a, b, and c display the 3D perspective views of the normalized force signal for the sample at different embedded depths as (a) $d = 0$, (b) $d = 20$, and (c) $d = 40$ nm, respectively. The tip is scanned at a fixed observation plane of $Z = 100$ nm.

The force patterns demonstrate a hollow right at the site of embedded dielectric structure, quite well related to the structure itself (a hollow). The electrostatic force signal becomes smallest when the tip is centered right with the sample structure. Since there is no polarization in the hollow, thus the electrostatic force exerting on the tip in the hollow region is reduced compared with other observation region beyond the hollow. The perturbed electrostatic force induced by the hollow is decreased when increasing the embedded depth, therefore, the signal contrast becomes worse. This is also due to the fast decaying feature of secondary electric field. The minimum normalized force signal at the three embedded depths is (a) $I_m = 0.83$,

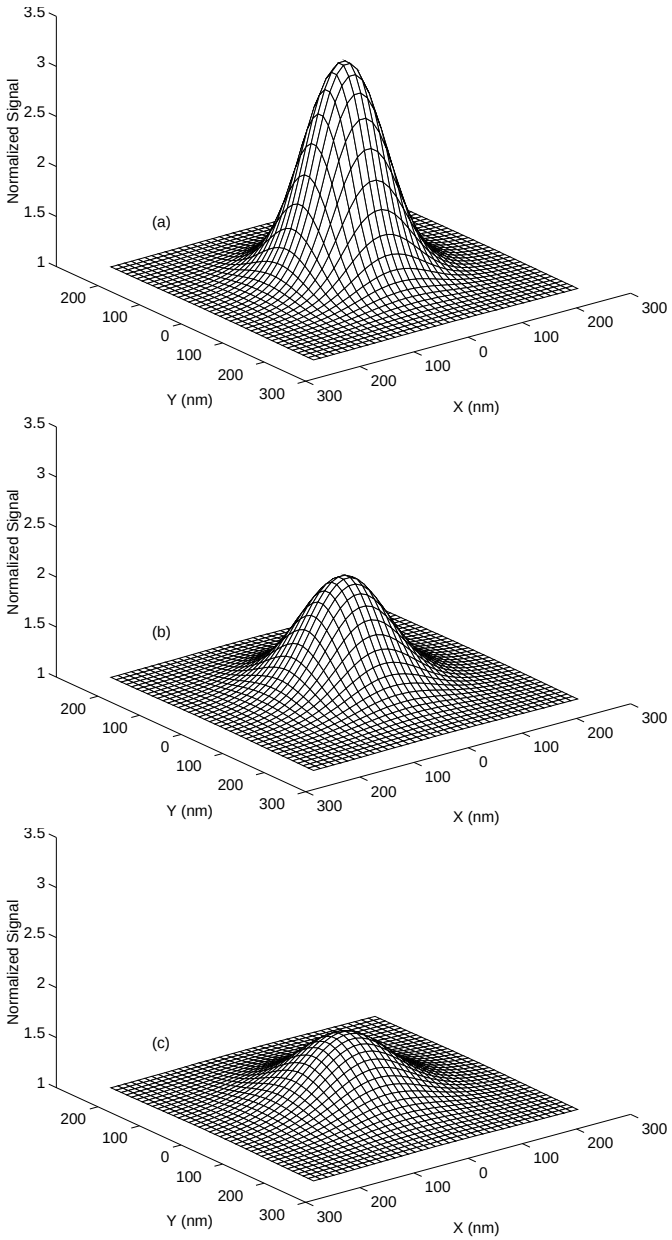

Fig. 2. 3D perspective view of the normalized force intensity $I = F/F_0$ for a cubic pad lying on the surface. The probe is scanned at different observation planes of (a) $Z = 175$, (b) $Z = 200$, and (c) $Z = 225$ nm. The pad has a dielectric constant of $\epsilon = 2.5$ and a sidelength of $a = 100$ nm.

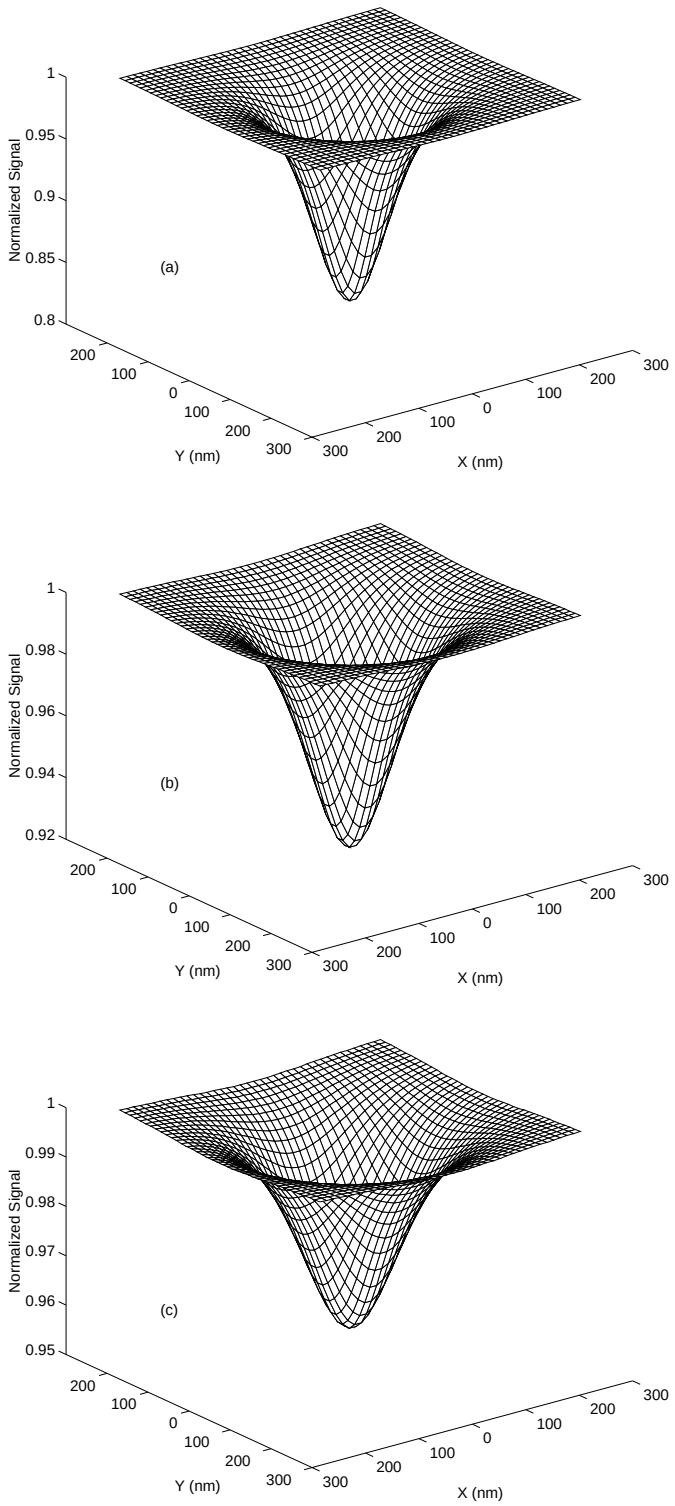

Fig. 3. 3D perspective view of the normalized force intensity $I = F/F_0$ for a cubic hollow (vacuum) embedded in the substrate. The probe is scanned at an observation plane of $Z = 100$ nm. The sidelength of hollow is $a = 100$ nm. The embedded depth of hollow is (a) $d = 0$, (b) $d = 20$, and (c) $d = 40$ nm, respectively. Note the three figures are ploted in the different scales of z-axis for a clarity of view.

(b) $I_m = 0.92$, and (c) $I_m = 0.96$. The extended region of the signal contrast increases with the increase of the embedded depth. The apparent size of the hollow sample grows approximately linearly with respect to the embedded depth (equivallently the vertical tip-sample distance). For three embedded depths it is about 140, 160, and 180 nm, respectively.

Although we only consider a hollow sample here, other embedded surface structure with a dielectric constant less than that of substrate medium should also exhibit a hollow character in the force pattern because the force is reduced by the negative polarization of sample $(\epsilon - \epsilon_s)\mathbf{E}(\mathbf{r})$.

On the contrary, an embedded structure with a larger dielectric constant than that of substrate medium should demonstrate a protrusion character in the force pattern, similar to the case of the topographic surface structure. This can be ascribed to the appearance of a positive polarization source $(\epsilon-\epsilon_s)\mathbf{E}(\mathbf{r})$. Such a qualitative prediction is verified by our numerical simulations.

We assume that a cubic pad is embedded below the surface and possesses a dielectric constant of $\epsilon = 5.0$. The 3D perspective views of the normalized force signal for the pad at different embedded depths as (a) $d = 0$, (b) $d = 20$, and (c) $d = 40$ nm are depicted in Figures 4a, b, and c, respectively. The tip is scanned at a fixed observation plane of $Z = 100$ nm. We can see that the force pattern indeed shows a protrusion right above the embedded structure. It implies a secondary field source at this site, which is a positive polarization. The force signal decays when the embedded depth and thus the vertical tip-sample distance increases. The maximum normalized force signal for three embedded depths are (a) $I_m = 1.12$, (b) $I_m = 1.06$, and (c) $I_m = 1.04$, respectively. The corresponding apparent size of the embedded pad is about 160, 180, and 200 nm, respectively.

The force signal for the embedded structure is much weaker compared with the force pattern shown in Figures 2a-c for the topographic surface structure. This can be attributed to the screened effect of the substrate medium to electrostatic interaction, which is related to the dielectric constant of substrate medium ϵ_s as well as the image factor $\gamma_2 = 2/(1 + \epsilon_s)$ (See Eqs. (12 14, 16, 22)). This screened effect decreases the local field inside the embedded pad, thus the secondary field induced by the polarization $(\epsilon-\epsilon_s)\mathbf{E}(\mathbf{r})$ is also greatly reduced. Therefore, the force signal is much weaker than that of the topographic structure, for which no screened effect exists. From this point of view, one can identify these two kinds of surface structures in terms of the measurement of SEFM, irrespective of the similarity between their force patterns.

The interference effect of signal between densely arranged sample particles appears in many kinds of scanning near-field microscopies, and results in complexity and confusion in interpreting the observed signal and correctly extracting the surface structure information.

To demonstrate the interference effect of force in SEFM quantitatively, we consider four closely arranged identical cubic pads with their center located at the apexes of a square. The sidelengths of each pad and the square are

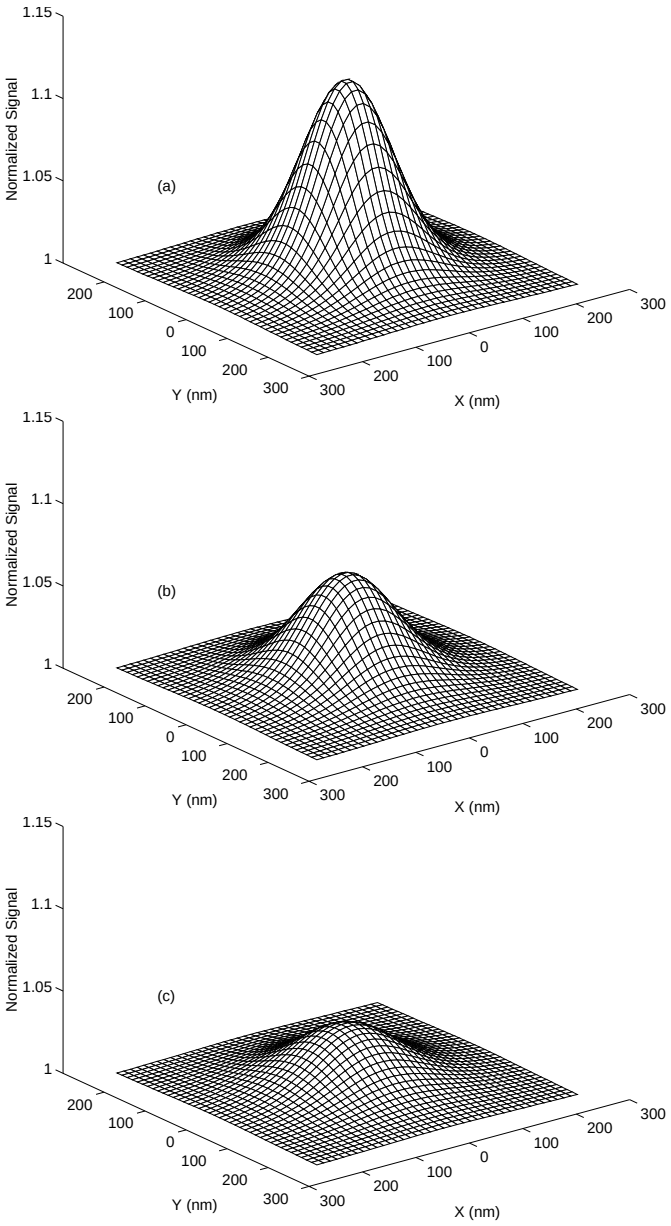

Fig. 4. 3D perspective view of the normalized force intensity $I = F/F_0$ for a cubic pad embedded in the substrate. The probe is scanned at an observation plane of $Z = 100$ nm. The pad has a sidelength of $a = 100$ nm and a dielectric constant of $\epsilon = 5.0$. The embedded depth of pad is (a) $d = 0$, (b) $d = 20$, and (c) $d = 40$ nm, respectively.

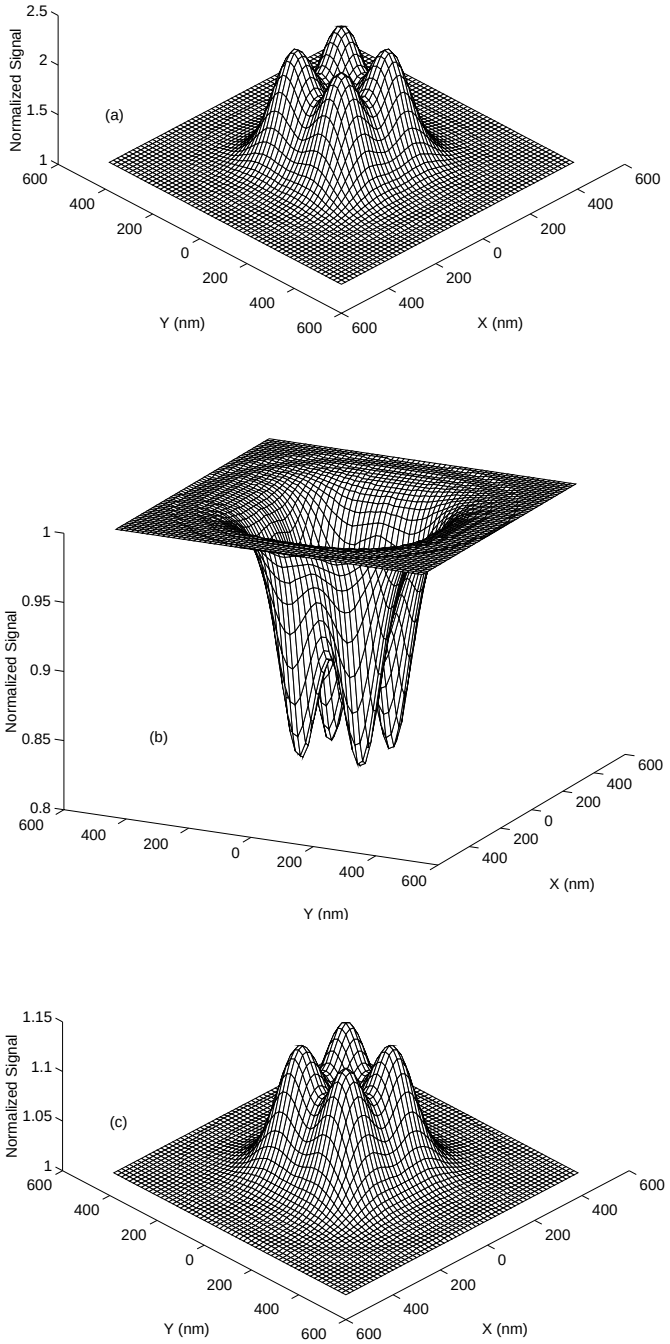

Fig. 5. 3D perspective view of the normalized force intensity $I = F/F_0$ for four identical cubic pads with their centers located at the apexes of a square. The sidelength of each pad and the square is 100 and 200 nm, respectively. (a) Topographic structure with a dielectric constant of $\epsilon = 2.5$. (b) Embedded hollow (vacuum) with an embedded depth of $d = 0$. (c) Embedded dielectric structure with a dielectric constant of $\epsilon = 5.0$ and an embedded depth of $d = 0$. The probe is scanned at an observation plane of (a) $Z = 200$, (b) $Z = 100$, and (c) $Z = 100$ nm, respectively.

100 and 200 nm, respectively. Figures 5a, b, and c display respectively the electrostatic force patterns for three kinds of surface structures: (a) topographic structure with a dielectric constant of $\epsilon = 2.5$; (b) embedded structure with a dielectric constant of $\epsilon = 1.0$ and an embedded depth of $d = 0$; (c) embedded structure with a dielectric constant of $\epsilon = 5.0$ and an embedded depth of $d = 0$. The corresponding observation planes are $Z = 200$, 100, and 100 nm, respectively. The force patterns seem to be very close to a simple superposition of the individual force signal

of four single pads, which has been shown in Figures 2b, 3a, and 4a.

Detailed data analysis follows that the force pattern of four pads is simply the superposition of the individual signal of each pad in all cases of surface structures . Thus it can be concluded that the interference effect in SEFM is not remarkable. This also implies that the coupling effect among various secondary field source is relatively weak. The field distribution around each pad changes very little in the presence of other pads. This phenomenon can be attributed to the fast decaying character of an electric field induced by the polarized sample in SEFM. The weak interference effect in SEFM is quite helpful for the retrieval of surface structure from the electrostatic force pattern.

4 Conclusions

We have applied a self-consistent method in a real-space representation to calculate the electric field distribution in a complex system composed of a conductive tip, sample, and substrate in SEFM, and evaluated the electrostatic force exerting on the tip. We consider two kinds of surface structures, one is the topographic structure lying on the surface, the other is the dielectric structure embedded in the substrate. For these two kinds of surface structure, the same technique of Green's function and standard image charge approach are combined to obtain a self-consistent integral equation, which is satisfied by a local electric field in the surface structure and can be solved numerically through a real-space discretization procedure. The simulation results show that the electrostatic force pattern can be well related to the surface structure. The force pattern for the topographic structure shows a protrusion around the surface structure. The force pattern for the embedded dielectric structure demonstrates a hollow around the structure with a dielectric constant less than that of substrate medium. On the contrary, it appears a protrusion around an embedded structure with a larger dielectric constant than that of the substrate medium, but such a force signal is much weaker than that of the topographic structure. Therefore, one can distinguish these surface structures from the analysis of the pure electrostatic force information in SEFM.

The interference effect of force is shown to be weak in the SEFM. The force signal of densely arranged dielectric pads is simply the superposition of individual force signal of each pad alone. This superior character can be of help to relate the force information to the surface structure apparently. The self-consistent approach has been proven to be effective in practice. The numerical calculations can provide detailed quantitative knowledge about the interaction between a charged tip and various kinds of surface structures, thus this approach is quite useful to solve the difficult inverse problem in SEFM, *i.e.*, to retrieve the surface structure through the pure electrostatic force information. However, more research works should be conducted for the complete solution of such an inverse problem owing to its complexity.

This work was supported by the National Natural Science Foundation of China.

References

1. G. Binnig, H. Rohrer, Ch. Gerber, E. Weibel, Phys. Rev. Lett. **49**, 57 (1982).
2. G. Binnig, C.F. Quate, Ch. Gerber, Phys. Rev. Lett. **56**, 936 (1986).
3. Y. Matin, C. Williams, H.K. Wickramasinghe, J. Appl. Phys. **61**, 4723 (1987).
4. J. Hu, X.-D. Xiao, D. Ogletree, M. Salmeron, Science **268**, 267 (1995).
5. J. Hu, X.-D. Xiao, M. Salmeron, Appl. Phys. Lett. **67**, 476 (1995).
6. H. Bluhm, A. Wadas, R. Wiesendanger, K.-P. Meyer, L. Szcześniak, Phys. Rev. B **55**, 4 (1997).
7. S. Watanabe, K. Hane, T. Ohye, M. Ito, T. Goto, J. Vac. Sci. Technol. B **11**, 1774 (1993).
8. M.F. Iskander, H.Y. Chen, J.E. Penner, Appl. Opt. **28**, 3083 (1989).
9. G.H. Goedecke, S.G. O'Brien, Appl. Opt. **27**, 2431 (1988).
10. *Near Field Optics*, NATO Advanced Study Institute, Series E: Applied Sciences, edited by D.W. Pohl, D. Courjon (Kluwer, Dordrecht, 1993), Vol. 242.
11. Z.Y. Li, B.Y. Gu, G.Z. Yang, Phys. Rev. B **55**, 10883 (1997).
12. Z.Y. Li, B.Y. Gu, G.Z. Yang, Phys. Rev. B **57**, 9225 (1998).
13. J.D. Jackson, *Classical Electrodynamics* (Wiley, New York, 1975), Chap. 2.
14. J.A. Stratton, *Electromagnetic Theory* (McGraw Hill, London, 1941), Chap. 3.